An overview of an experimental campaign for arrays of wave energy conversion systems

Nicolás Faedo, Yerai Peña-Sanchez, Edoardo Pasta, Guglielmo Papini, Facundo D. Mosquera and Francesco Ferri

Abstract—**Among the main challenges to overcome towards the large-scale commercial exploitation of wave energy systems, the deployment of arrays of wave energy converters (WECs) is of crucial importance. In the path towards a successful installation of multiple devices, the development of representative and reliable numerical models for dynamical analysis, performance assessment, and optimal definition of the layout configuration, is a fundamental step. To test the reliability of a model, experimental results are crucial assets for the process of model validation. Given the absence of available experimental data concerning arrays of WEC systems, we describe, in this paper, an experimental campaign fully conducted with the sole objective of generating and providing an open-access dataset on WEC farms: SWELL [1]. Such dataset is composed by four different categories of tests (free surface elevation in undisturbed wave tank, blocked device for wave contribution measurement, uncontrolled and controlled motion), and all the main motion and force variables are provided in the different regular and irregular wave conditions. In the attempt of enabling an informed and simple usage of the dataset, this paper provides a clear description of the test design and implementation.**

Index Terms—**Wave energy, Arrays, Modelling, Validation, Experimental testing**

I. Introduction

THE potential of ocean renewable energies in the pathway towards a low-carbon energy society is widely recognised globally, generating significant interest from a plethora of entities [2]–[4]. In particular, within the field of ocean renewables, the vast energy potential from ocean waves, *i.e. wave energy*, remains largely untapped. Estimations indicate that wave energy offers an exploitable power resource of 30.000 [TWh/year] [2]–[4], making it a substantial contributor to the energy mix. Compared to solar and wind power, wave energy has a higher density [5], is consistently available up to 90% of the time [6], highly predictable [7], and has a negligible impact on the environment when harvested properly [8], [9].

Nonetheless, availability of commercially viable wave energy harvesters remains challenging [10]. This difficulty can be attributed to various factors, including the diverse and unpredictable nature of wave resources in different locations worldwide, the demanding requirements for survivability in a hostile environment, and the lack of consensus on the optimal design and concept of wave energy converters (WECs). As a result, the levelised cost of energy (LCoE) for wave energy is higher compared to other renewable energy sources, which hampers the widespread commercialisation of WEC systems [10], [11].

Within the field, it is widely recognised that reducing the LCoE and achieving widespread commercialisation of wave energy depend on two fundamental factors. The first crucial element involves the utilisation and advancement of appropriate control system technology, which can optimise the energy extraction from wave resources while considering the device inherent physical limitations [12], [13]. The second key factor in reducing the LCoE, along with the suitable control technology, is the deployment of WEC systems in array configurations, commonly known as "parks" or "farms." This approach aims to minimise the costs associated with installation, operation, and maintenance per device, ultimately meeting the capacity requirements [14]–[17].

Mathematical models play an indispensable role in advancing the commercialisation of WEC systems, by providing valuable insight into the behavior of WECs under specific operating conditions. However, the reliability of these models is always a significant concern, as they need to accurately represent reality in order to support development stages and facilitate decision-making [16], [17]. To ensure the reliability of a model, experimental results are invaluable for validation purposes. Additionally, the availability of experimental data opens up opportunities for data-based modelling of WEC systems, where real-world information is directly incorporated into the modelling process, akin to system identification techniques [18].

Recently, the so-called *SWELL* (Standardised Wave Energy converter array Learning Library) dataset has been presented in [1], constructed on the basis of four different main tests, comprising an approximate total of $\sim$3000 variables and more than $\sim 10^8$ datapoints, for up to 5 devices in 9 diverse WEC array layouts with different levels of interaction, and 19 carefully selected operating conditions (featuring regular, bimodal, irregular, and white noise sea states). Such a dataset is generated as part of a larger experimental campaign, conducted in the wave tank facilities available at Aalborg University (Denmark), using a small-scale (1:20) Wavestar-like [19] prototype as the baseline device, as

N. Faedo, E. Pasta, and G. Papini are with the Marine Offshore Renewable Energy Lab, Department of Mechanical and Aerospace Engineering, Politecnico di Torino, Torino, Italy (Corresponding author: N. Faedo - nicolas.faedo@polito.it).

Y. Peña-Sanchez is with the Department of Mathematics, University of the Basque Country, Leioa, Spain.

Facundo D. Mosquera is with the LEICI, Universidad Nacional de La Plata, La Plata, Argentina.

Francesco Ferri is with the Department of the Built Environment, Aalborg University, Aalborg, Denmark.

Digital Object Identifier:
https://doi.org/10.36688/ewtec-2023-379

depicted in Figures 1 and 3, effectively featuring an electric (direct drive) PTO system.

This paper presents an overview of the experimental campaign involved in the development of SWELL, making specific emphasis in the different tests and their corresponding synergy. Particularly, SWELL encompasses four distinct tests, aimed at generating comprehensive data for model validation and data-based modelling tasks in the field of WEC systems. These tests encompass a wide range of key variables, including free-surface elevation at strategic points within the basin, wave excitation force (force induced by the waves), uncontrolled motion, and device behavior under energy-maximising control. The dataset, to the best of our knowledge, represents the most extensive collection characterising arrays of WEC systems currently available in the literature.

The remainder of this paper is organised as follows. Section II details the experimental setup considered, including wave tank facilities, baseline prototype and instrumentation, and layout configurations. Section III offers a detailed account of the sea states (operating conditions) considered, and the underlying criteria adopted for their choice within the experimental campaign. Section IV provides an account of each test performed, including sample results to illustrate the dataset. Section V discusses the ordering and structure of SWELL, with specific reference to each of the variables present within the dataset, and their connection with the tests performed. Finally, Section VI encompasses the main conclusions of this experimental campaign and the development of SWELL.

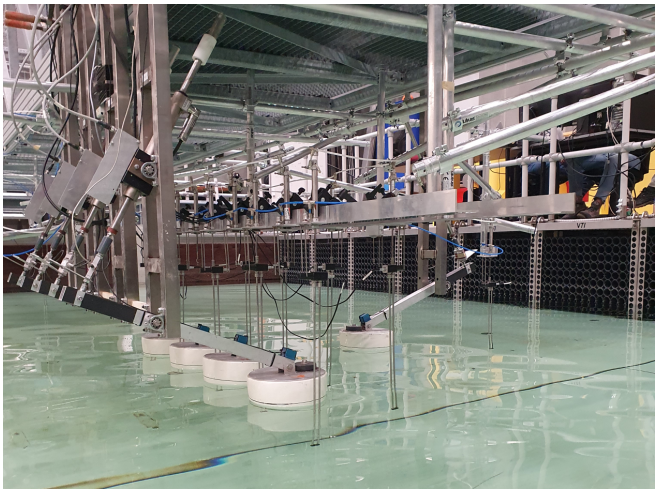

Fig. 1. Photographs of the experimental setup designed for the WEC array experimental campaign, from different angles.

II. Experimental setup and layout design

This section is dedicated to provide a detailed description of the experimental setup considered, as presented in Figure 1, including the Aalborg University wave tank specifications, baseline WEC system, equipment associated with each device and characterisation of PTO systems, WEC and wave gauges disposition within the wave tank, and considered array layout specifications. For the latter, we provide explicit motivation for the choice of each layout considered, with emphasis on specific aspects which are fundamental within validation/data-based modelling activities.

A. Wave tank specifications

The experimental campaign wave tank facilities, used to achieve the objectives and generate the dataset SWELL in [1], are located at the Ocean and Coastal Engineering Laboratory in Aalborg University, Denmark. The basin dimensions are described in the schematic shown in Figure 2. Specifically, the available facilities consist of a basin measuring 19.3 meters in length, 14.6 meters in width, and 1.5 meters in depth, with an active test area of 13 meters in length and 8 meters in width. The wave tank is equipped with a state-of-the-art wavemaker system, custom-made by VTI [20], which features a long-stroke segmented design with 30 individually controlled wave paddles. This advanced system enables the generation of various sea state conditions with high precision and incorporates active absorption capabilities.

For this study, the water depth in the tank is fixed at 0.9 meters, while the wavemaker is set to produce long-crested waves parallel to the x-axis and with a direction of 0 degrees along the y-axis, as depicted in Figure 2. In addition to the active absorption provided by the wavemaker system, the basin is equipped with passive wave absorption elements made of stainless steel and hot galvanised stretch metal sheets.

B. Prototype WEC and acquisition system

The selected WEC system for this array experimental campaign is a scaled version (1:20) of the Wavestar wave energy conversion system [19]. A representation of a single unit of this prototype can be seen in Figure 3. The system consists of a floater that is mechanically hinged to a fixed reference point above the water surface, denoted as point **A** in Figure 3. When in the equilibrium position, the floater arm is inclined at approximately 30 degrees relative to the still water level (SWL). It is important to note that the WEC is capable of motion in a single degree of freedom (DoF).

The power take-off (PTO) system utilised is an electrical, direct-drive, linear motor *LinMot Series P01-37 x 240F*. It is positioned at the upper structural joint of the device, as illustrated in Figure 3. The corresponding drive for the PTO is the *LinMot E1200*, which has a force rating of up to +/- 200 N.

To ensure redundancy, the translational displacement of the PTO system is measured not only by the PTO driver itself but also with a dedicated laser position sensor - *MicroEpsilon ILD-1402-600*. Additionally, the total force applied to the PTO axis is measured using a *S-beam Futek LSB302* load cell. The WEC system is also equipped with a dual-axis accelerometer, specifically the *Analog Devices ADXL203* sensor, which is positioned on top of the prototype floater. Alongside the translational motion measurements, this accelerometer is utilised to derive measurements of rotational motion, such as angular displacement and velocity, about the

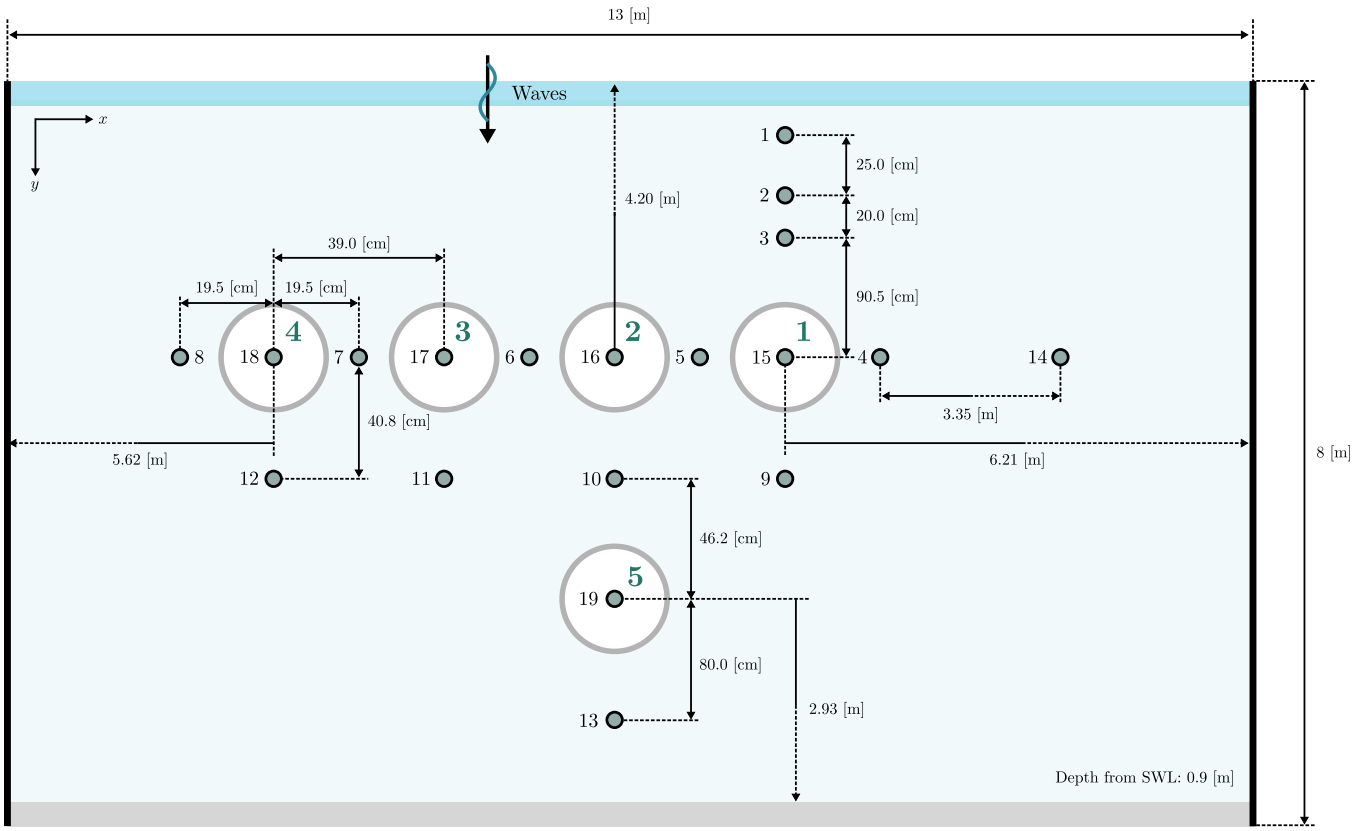

Fig. 2. Schematic representation of the wave basin at the Ocean and Coastal Engineering Laboratory, in Aalborg University [1].

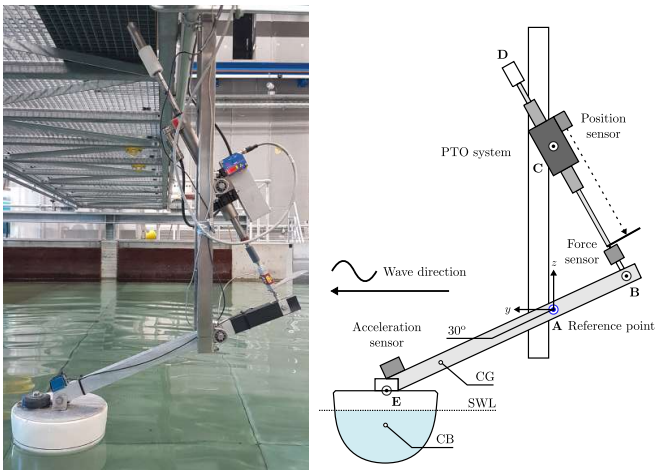

Fig. 3. Photo of the baseline Wavestar prototype unit for the WEC array experimental campaign (left) and associated schematic representation (right). The acronym SWL stands for still water level.

corresponding fixed reference point. We further note that data acquisition is consistently performed at a sampling rate of 200 [Hz], for all the acquired variables within the totality of the experimental campaign.

C. Wave gauges and devices positioning

The measurement of free-surface elevation is accomplished using resistive-type wave probes. In this experimental campaign, a total of 19 wave probes (WP) have been utilised and strategically positioned within the wave tank, as illustrated in Figure 2.

Regarding device positioning, a total of 5 prototypes (D1 to D5) are considered in this WEC array experimental campaign. Each device is mounted on a gantry through a supporting structure, as depicted in Figure 1. Devices D1 to D4 are arranged in a row-like formation with a center-to-center distance of 39 cm. This distance corresponds to approximately 1.5 times the diameter of the prototype floater, resulting in an inter-device distance (edge-to-edge) of approximately 1 radius, equivalent to 13 cm. Each device can be manually lifted out of the basin, allowing for the testing of different layout configurations by removing devices from the water. Notably, D5 is mounted on the rear side of the gantry and is positioned in a "flipped" orientation compared to devices D1 to D4. This specific arrangement is designed to create a heterogeneous array configuration, enriching the results and the associated dataset. Consequently, the response of D5 will naturally differ from that of D1-D4.

D. Array layout design

A total of 9 distinct layout configurations (L0 to L8) are studied within [1], that involve simultaneous operation of up to 5 different devices within the wave tank, as illustrated schematically in Figure 4. The selection of these layouts is not arbitrary and is based on specific considerations, as detailed below.

The testing set comprises two layouts with a single device (L0 and L8), three layouts with two devices (L1 to L3), two layouts with three prototypes (L4 and L5), and finally, one layout each with 4 and 5 WECs operating within the basin (L6 and L7, respectively).

The baseline layout, L0, which has been previously studied in the literature for this specific Wavestar pro-

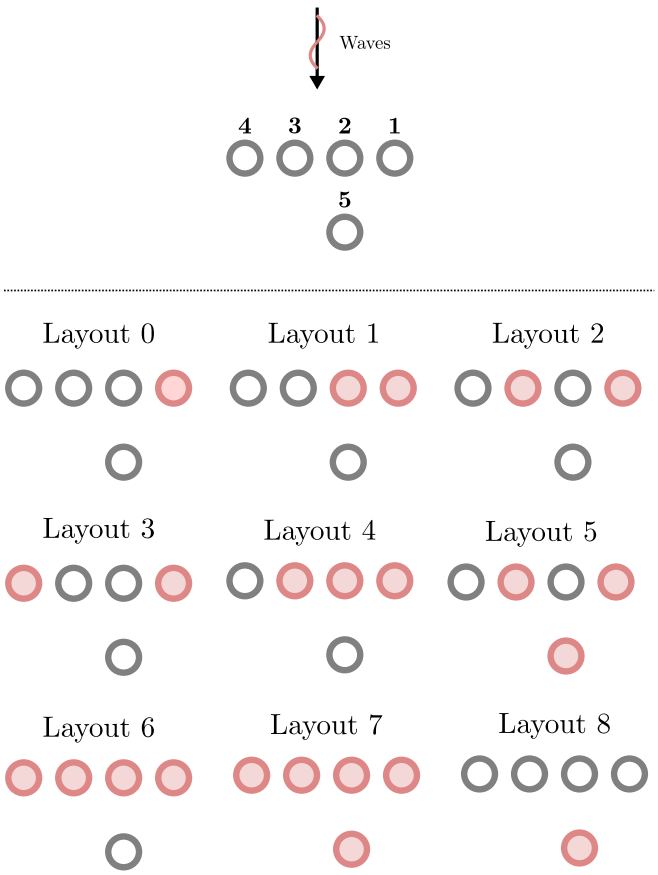

Fig. 4. Full set of layouts considered within the WEC array experimental campaign presented in this study.

totype [21]–[24] and discussed in Section I, consists of a single device configuration. Layout L8, on the other hand, is designed to specifically characterise the heterogeneity among devices, and is considered in a standalone fashion. Layouts L1 to L3 form the first set of layouts with more than a single WEC prototype. These layouts have a similar formation but with different inter-device distances. The design of L1 to L3 allows for a direct assessment of the effects of device interactions as a function of the distance between the bodies. Understanding these constructive and destructive effects within WEC array configurations has been proven to be essential for optimal layout design and control [25]–[28]. Layouts L4 and L5 introduce a third device into the basin and serve as a natural extension of L1 and L2. While L4 includes a device positioned between D1 and D3 in a row-like formation, L5 forms a triangle-like shape by incorporating D5 into the wave tank. Layout L6 represents a four-device row formation, incorporating all the devices used in L0 to L4, namely D1 to D4. Lastly, L7 represents the most complex case in terms of modelling and configuration, involving all 5 devices operating simultaneously within the basin.

III. Definition of Sea States

In this section, we provide a description of the sea states that have been considered in the experimental campaign. The selection of these sea states is motivated by their relevance for different modelling and validation tasks. A total of 12 sea states are included, with the number of realisations (#R) varying depending on the specific operating condition. The sea states can be categorised into four types within the SWELL database:

- *Regular sea state* (RSS): These sea states involve the generation of waves with a monochromatic spectrum, meaning that they are deterministic and consist of a single component at a specific frequency.
- *Bimodal sea state* (BMSS): These sea states also have a deterministic nature and are generated with a bichromatic spectrum. They consist of two selected components in terms of frequency.
- *Irregular sea state* (ISS): These sea states are represented by a stochastic approach. Specifically, JONSWAP spectra [29] are considered in this study, as discussed further in Section III-C.
- *White noise sea state* (WNSS): These sea states are generated based on a constant spectral density within a predefined frequency range.

These different types of sea states provide a comprehensive range of wave conditions for the experimental campaign.

TABLE I
Waves tested within the presented experimental campaign.

ID	Type	Period [s]	Height [m]	γ	#R	Length [s]
RSS1	Regular	0,8	0,05	-	1	60
RSS2	Regular	0,9	0,05	-	3	60
RSS3	Regular	1	0,05	-	1	60
RSS4	Regular	1,2	0,05	-	3	60
RSS5	Regular	1,5	0,05	-	1	60
BMSS	Bimodal	{0.9, 1.2}	Equal energy	-	1	60
ISS1	Irregular	1,412	0,063	3,3	2	300
ISS2	Irregular	1,836	0,104	3,3	2	300
ISS3	Irregular	0,988	0,0208	1	2	300
WNSS1	W. noise	[0.5, 10]	0,01	-	1	300
WNSS2	W. noise	[0.5, 10]	0,03	-	1	300
WNSS3	W. noise	[0.5, 10]	0,05	-	1	300

Total number of waves tested: 19

A. Regular sea states

Five different regular wave conditions (RSS1 to RSS5) are considered. These wave conditions have strategically selected frequency components with respect to the device response and have a constant wave height. Figure 5 (first figure from the top) shows the theoretical spectrum associated with each RSS condition (solid lines), normalised relative to the spectrum with the highest energy, for illustrative purposes. The dashed line in Figure 5 represents the magnitude of the torque-to-motion frequency-response map for the baseline Wavestar prototype system described in Section II-B. This response map is computed using a Boundary Element Method (BEM) solver (specifically, the open-source software Nemoh [30]).

The selection of these regular wave conditions aims to cover the typical operational range of the Wavestar system, including resonance (RSS2), low-frequency (RSS3, RSS4, and RSS5), and high-frequency (RSS1) behavior. Different numbers of realisations (#R) have been considered for each RSS condition, depending on their specific characteristics. While these sea states are deterministic, multiple realisations have been generated for a subset of these conditions to provide

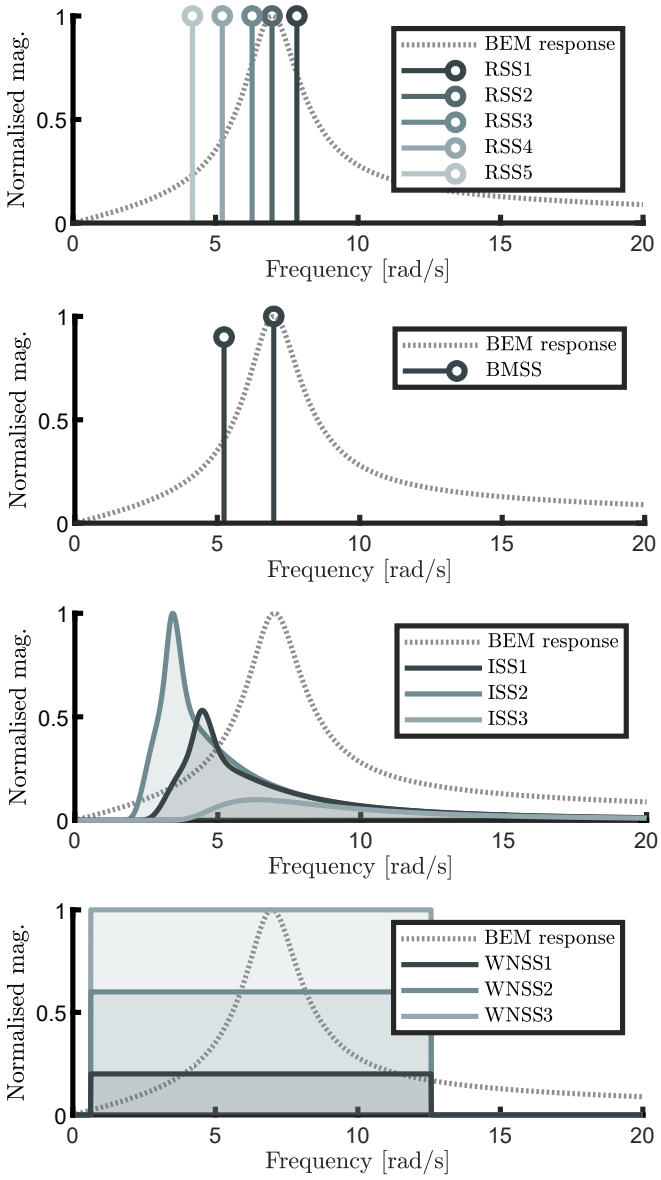

Fig. 5. Theoretical spectra for the wave conditions used within this experimental study.

information about the wavemaker systes capability to reproduce a given sea state in different runs. A constant wave height has been chosen for these regular wave conditions to ensure comparability. The specific wave height is determined by considering any limitations associated with the wave generation system, which can accurately generate waves within the basin up to a certain height limit based on the wave period.

B. Bimodal sea state

Bimodal sea states are an extension of regular wave conditions as they incorporate (in a deterministic fashion) an additional frequency component. These sea states, which are typically associated with a combination of wind and swell seas, can be used in modelling/system dynamics to investigate nonlinear behavior. For example, they can be used to assess the validity of the principle of superposition for specific frequency components, or to estimate the class of functions characterising the nonlinearities of the WEC.

In this experimental campaign, a single bimodal sea state (BMSS) is considered. This sea state consists of one frequency component placed at the resonance behavior of the WEC prototype (equivalent to RSS2) and a low-frequency contribution (equivalent to RSS4). The theoretical spectrum of the BMSS has been characterised using an equal energy method, as shown in Figure 5 (second figure from the top), where the spectrum is normalised relative to the frequency component chosen at the system resonance.

C. Irregular sea states

As is common in the marine/ocean engineering community, realistic waves are often represented using stochastic descriptions with an associated dense spectrum (see *e.g.* [31]). Among the various models used to characterise ocean waves, the JONSWAP spectrum [29] is a widely employed representation for wind-generated seas with fetch limitations. In this stochastic description, three main parameters can be identified: the significant wave height H_s, the peak wave period T_p, and the peak-enhancement factor γ.

This experimental campaign comprises three irregular sea states (ISS1 to ISS3) as described in Table I. These sea states have been selected based on the benchmark control case established by the WEC^{3}OMP [21] and aim to represent various operational conditions for both uncontrolled and controlled device motion. The theoretical spectra associated with these sea states, normalised with respect to ISS2, are illustrated in Figure 5 (third figure from the top). ISS1 and ISS2 represent narrow-band conditions with different peak periods and significant wave heights. On the other hand, ISS3 represents a wide-banded operating case with energy content across low, resonance, and high-frequency components. To ensure a diverse representation of each operating condition in the time domain, two different realisations are considered for each ISS in the dataset.

D. White noise waves

Whilst irregular sea states can effectively represent realistic wave conditions, they may not be entirely suitable for certain purposes, such as control-oriented modelling and validation. This is due to the fact that WEC systems are required to operate in a potentially wide range of sea states, each with its own spectral content and characteristics. Consequently, modelling and validating WEC controllers for diverse operating scenarios can be challenging and time-consuming, particularly when relying on a limited number of irregular sea state tests.

To overcome this challenge, this experimental campaign incorporates sea states described in terms of white noise spectra. These sea states are characterised by a constant spectral density function within a sufficiently large, yet bounded, frequency range. The chosen frequency range must be extensive enough to adequately cover the typical operating conditions of WECs, ensuring that the associated dataset is representative of a wide array of operating scenarios.

In this experimental campaign, we specifically include three different white noise sea states (WNSS1 to WNSS3), as outlined in Table I and depicted in Figure 5 (fourth figure from the top). These sea states exhibit a constant frequency range that encompasses the primary dynamics of the baseline WEC prototype. However, their energy content progressively increases across WNSS1, WNSS2, and WNSS3. By varying the energy content, we aim to investigate how the system response is influenced by higher energy levels, which manifest as larger free-surface elevation fluctuations over time. This approach enables the gathering of data on any significant nonlinear behavior exhibited by the WEC prototypes, specific to each tested layout.

IV. Tests design and sample results

After providing the details of the baseline prototype and array layouts in Section II and discussing the chosen sea states for the SWELL experimental campaign in Section III, we now delve into a thorough description of the specific tests conducted and their inherent nature and interrelation. Four distinct tests are devised, involving either all or a subset of the selected sea states and WEC array layouts:

Test 1 *Free-surface elevation*: This test aims to capture the time-domain wave elevation signal at designated probe locations for each sea state and realisation employed in the experimental campaign. It is important to note that, as explained in Section IV-A, this test is independent of the array layout configurations outlined in Section II-D, *i.e.* is performed in abscence of devices within the tank.

Test 2 *Wave excitation*: The objective of this test is to determine the wave excitation force/torque corresponding to each generated free-surface elevation for the various sea states, realisations, and WEC array layouts specified in Section II-D.

Test 3 *Uncontrolled device motion*: In this test, the uncontrolled motion of the WEC device (displacement, velocity, and acceleration) is measured in relation to each generated free-surface elevation. It encompasses the different sea states, realisations, and WEC array layouts described in Section II-D.

Test 4 *Controlled device motion*: This test focuses on the controlled motion of the WEC device (displacement, velocity, and acceleration) in response to each generated free-surface elevation. It covers the various sea states, realisations, and WEC array layouts outlined in Section II-D.

Each test, as illustrated in Figure 6, is explained in dedicated sections (Sections IV-A to IV-D) following this paragraph, showcasing a number of example cases.

A. Test 1: Free-surface elevation

This test aims to generate time-series data of the free-surface elevation for each sea state (and realisation) listed in Section III within the SWELL experimental setup. Measurements are taken at various spatial points within the wave tank, as described in Section II-C. It is important to note that no device is present in the tank during this particular test. Wave probes WP 15, 16, 17, 18, and 19 are used to measure the free-surface elevation at the center point of each WEC system when it is in operation (refer to Figure 2).

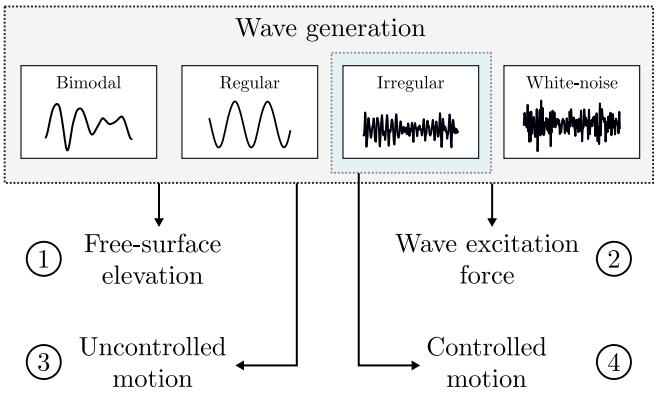

Fig. 6. Tests comprising the experimental campaign for the generation of SWELL.

To demonstrate the corresponding measurement of free-surface elevation, Figure 7 displays time-traces obtained from WP 1 for RSS2, RSS4 and BMSS, along with the corresponding magnitude of their fast Fourier transform (FFT). Furthermore, Figure 8 showcases measurements obtained by WP 1 for ISS2-1, and the white noise wave conditions (WNSS1). Qualitatively, a good agreement can be appreciated between measured data and theoretical spectrum, for all the cases analysed.

B. Test 2: Wave excitation

Following Test 1, as described in Section IV-A, the next step within this campaign is to measure the wave excitation force/torque acting on the various WEC array configurations for each specific free-surface elevation generated in the wave tank. To accomplish this, the devices in each layout are effectively blocked by locking the associated PTO motor shafts (as described in [18]). Consequently, the force exerted by the particular wave can be directly measured using the load cell attached to point **B** (refer to Section II-B and Figure 3). The measured force is then converted to torque with respect to point **A** using standard geometric relations.

To provide a brief illustration of the obtained measurements in this test, Figure 9 displays the wave excitation torque (computed about the corresponding reference point **A** in Figure 3) for L4 (consisting of D1, D2, and D3) and L5 (composed of D1, D3, and D5) when the generated wave corresponds to RSS4. It is evident that while the excitation is relatively similar for all devices in L4, while there are noticeable (phase) differences when considering L5 due to the positioning of D5 within the wave tank.

C. Test 3: Uncontrolled device motion

Test 3, introduced in this section, complements the information gathered from Tests 1 and 2 by providing motion variables for each device within SWELL, for every layout tested and each generated wave in the basin. Specifically, as described in Section II-B, two primary

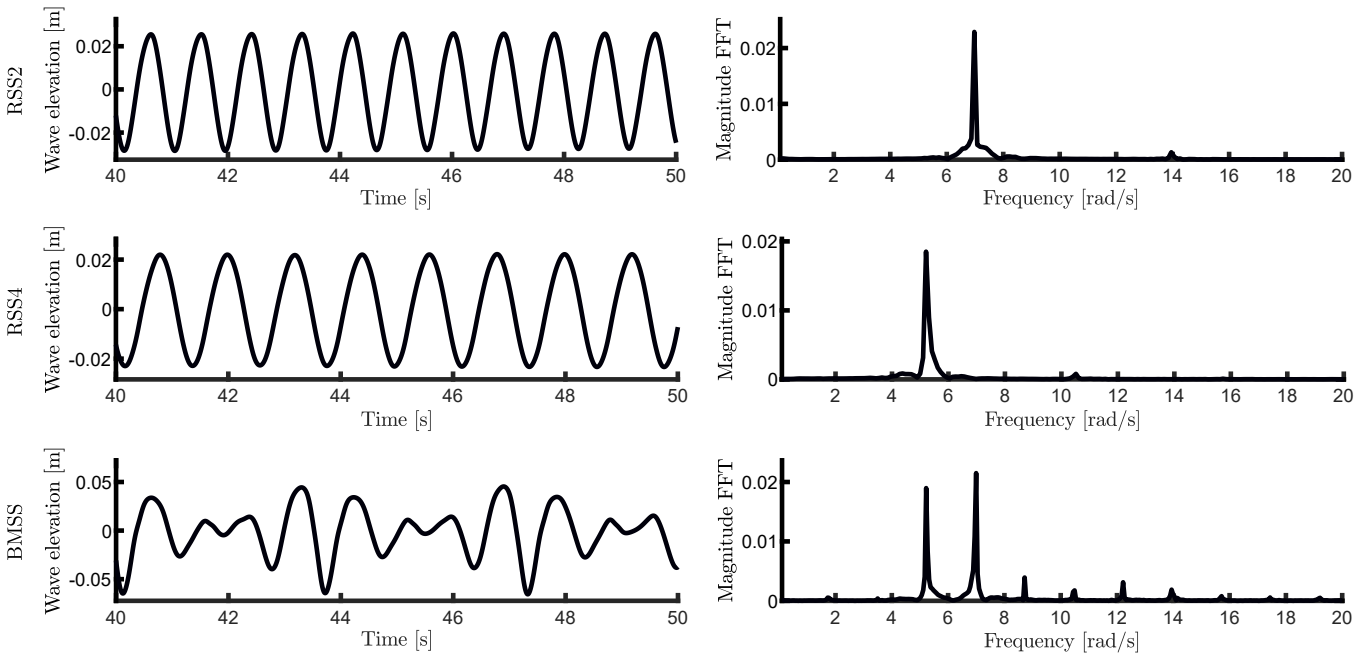

Fig. 7. Test 1: Regular and bimodal free-surface elevation measured by WP 1, in time (left), and frequency (right). Adapted from [1].

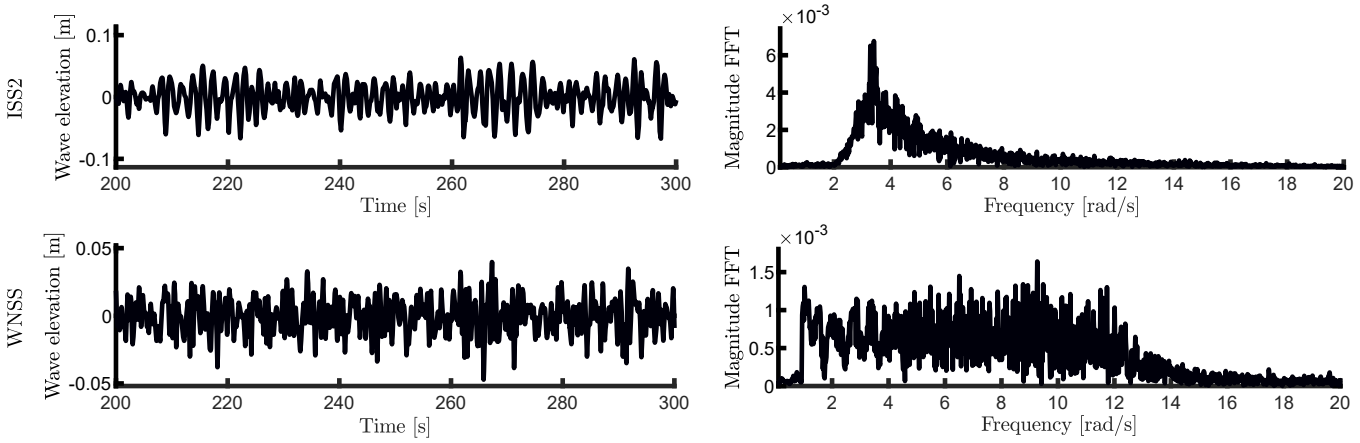

Fig. 8. Test 1: Irregular and white-noise free-surface elevation measured by WP 1, in time (left), and frequency (right). Adapted from [1].

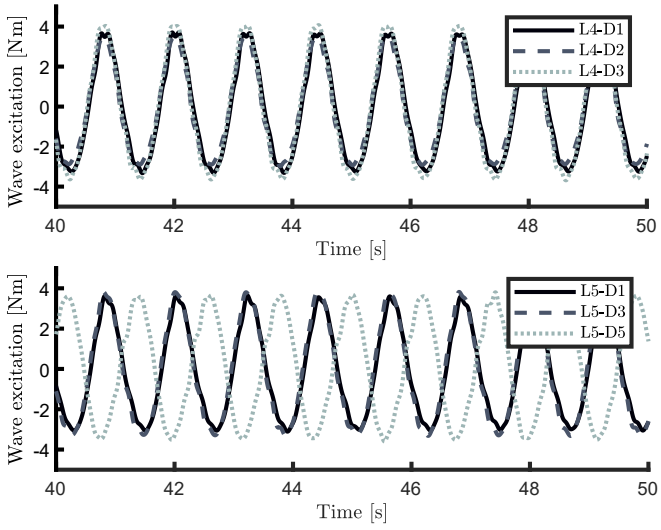

Fig. 9. Wave excitation torque for L4 and L5, when RSS4 is generated within the wave basin [1].

motion variables can be directly measured using the available instrumentation in each device: linear (PTO) position (either through the built-in sensor in the corresponding driver or the laser position sensor placed on top of the motor, as explained in Section II-B), and floater (linear) acceleration (measured using the accelerometer placed on top of each floater).

To briefly demonstrate the data collected from Test 3, Figure 10 shows angular positions $\theta_{\mathbf{A}}$ for each device in L4 and L5 when generating RSS4 in the wave basin. It is worth noting that this figure complements Figure 9, as it represents the motion of the WEC prototypes when the torque is applied to each array configuration. Interestingly, for this specific wave (RSS4), the devices in L4, arranged in a row-like formation, move synchronously with virtually the same amplitude and phase.

D. Test 4: Controlled device motion

Validated models, which accurately represent WEC systems operating under energy-maximising control,

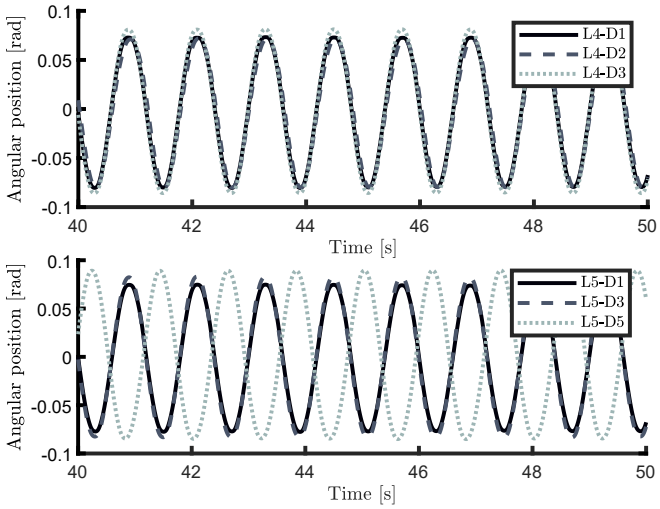

Fig. 10. Motion for L4 and L5, when RSS4 is generated within the wave basin [1].

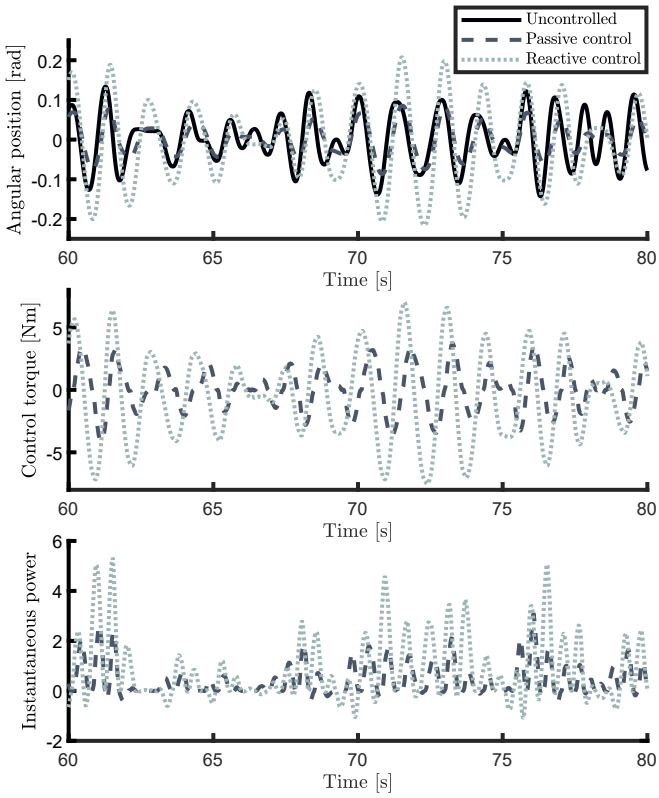

Fig. 11. Controlled behaviour for L0 when ISS1-1 is generated within the basin [1].

are crucial for precise performance evaluation of both individual systems, and array configurations. Considering this, Test 4 incorporates information into SWELL regarding a subset of the WEC layouts and sea states examined in this campaign, under various control conditions. Specifically, two well-established and widely adopted control architectures, commonly known as *passive* (proportional - P) and *reactive* (proportional-integral - PI) controllers, are considered. The parameters for these controllers are computed based on the impedance-matching condition (also referred to as complex-conjugate condition in the literature) for WEC systems, leveraging the frequency-response map of L0 (a single device - D1) as a reference point.

To illustrate the results obtained within this test, Figure 11 presents motion for L0, in uncontrolled (solid), passively- (dashed), and reactively-controlled (dotted) conditions, for ISS1-1. As it can be appreciated, both passive and reactive cases clearly present different closed-loop dynamics, with the latter generating both larger control torque requirements, and effective device motion, in line with the discussion provided within the first paragraph of this section (see also Section I). Note that, clearly, the reactive controller requires negative instantaneous power flow, injecting energy into the WEC system at specific time instants to maximise the total absorbed power [12].

V. Dataset specification

This section focuses on providing a description of the dataset SWELL, which consists of the data collected in the tests discussed in Section IV. The structure of the directory associated with SWELL can be seen in Figure 12. There are two main folders within the structure: ”Tests” and ”Linear motors”. The ”Tests” folder contains the core of the dataset, including data from Tests 1 to 4 (as described in Section IV) for each WEC array layout tested. On the other hand, the ”Linear motors” folder contains data related to each PTO linear motor, including friction and I/O tests. A description of the former can be found in [1].

SWELL consists entirely of files that are compatible with MATLAB, using the native ”.mat” format. This ensures that the dataset can be readily processed and analysed. The data is stored in a standard matrix format, eliminating any potential compatibility issues between different versions/releases of MATLAB. It is worth noting that ”.mat” files can also be easily opened using other tools such as Python or Octave, making them compatible with a wide range of software.

We describe, in the following, the main section of the directory, *i.e.* the ”Tests” folder. It contains nine subfolders, each corresponding to one of the nine tested layouts (L0 to L8). Within each of these folders, there are 19 ”.mat” files, each linked to a specific operating condition, representing a sea state and realisation (if applicable). For example, ”01_RSS1_1.mat” refers to the results for the first realisation of RSS1, while ”16_ISS3_2.mat” corresponds to ISS3, realisation 2.

Table II provides a comprehensive list of variables, including test, file name, description, units, and dimensions associated with each variable. The dimensions of the variables depend on the length of the time vector (N_t) and the number of devices (N_d) in the layout. The time vector, as specified in Table II, is consistent across all tests and variables. In other words, all variables have been synchronised and interpolated based on a single reference time vector for each ”.mat” file within the main ”Tests” folder. This synchronisation is made possible by utilising a trigger output signal provided by the wavemaker system at Aalborg University, which marks the precise start and end of wave generation. Additionally, the signals have been filtered to eliminate noise in the dataset. To achieve this, a zero-phase

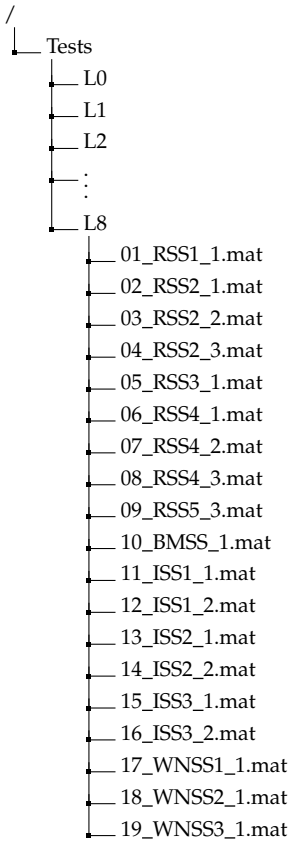

Fig. 12. Directory structure for SWELL.

(forward-backward) Chebyshev filter, with a filter order of 4 and a sufficiently large cut-off frequency of 50 [rad/s], has been applied to all variables listed in Table II.

VI. Conclusions

In this paper, we present a comprehensive description of an experimental campaign conducted with the primary aim of providing an open-access dataset for wave energy conversion (WEC) system arrays, known as SWELL. This dataset serves as a valuable resource for model validation and data-driven modelling within the WEC development community. Four main tests have been included as part of the campaign, strategically designed to capture key variables relevant to WEC systems. These variables include free-surface elevation at various locations in the wave basin (Test 1), wave excitation force (Test 2), uncontrolled motion (Test 3), and system behavior under energy-maximising control conditions (Test 4), using both passive and reactive control approaches. The dataset incorporates these variables for different sea states, devices, and set of layouts considered.

To the best of our knowledge, SWELL represents the most extensive open-access dataset available in the literature for characterising arrays of WEC systems. It encompasses a wide range of WEC layouts, realistic PTO effects (including energy-maximising control), and diverse testing scenarios following a consistent protocol. This dataset caters to the needs of various modelling tasks, providing a vital resource for assessing the reliability of different numerical modelling approaches. In this way, we strongly believe SWELL has the capabilities for supporting efficient decision-making processes, hence contributing to the advancement of ocean wave energy towards successful commercialisation.

References

[1] N. Faedo, Y. Peña-Sanchez, E. Pasta, G. Papini, F. D. Mosquera, and F. Ferri, "SWELL: an open-access experimental dataset for arrays of wave energy conversion systems," *Renewable Energy*, 2023.

[2] G. Mork, S. Barstow, A. Kabuth, and M. T. Pontes, "Assessing the global wave energy potential," in *International Conference on Offshore Mechanics and Arctic Engineering*, vol. 49118, 2010, pp. 447–454.

[3] K. Gunn and C. Stock-Williams, "Quantifying the global wave power resource," *Renewable Energy*, vol. 44, pp. 296–304, 2012.

[4] B. Reguero, I. Losada, and F. Méndez, "A global wave power resource and its seasonal, interannual and long-term variability," *Applied Energy*, vol. 148, pp. 366–380, 2015.

[5] M. E. McCormick, *Ocean wave energy conversion*. Courier Corporation, 2013.

[6] I. López, J. Andreu, S. Ceballos, I. M. De Alegría, and I. Kortabarria, "Review of wave energy technologies and the necessary power-equipment," *Renewable and sustainable energy reviews*, vol. 27, pp. 413–434, 2013.

[7] W. Sasaki, "Predictability of global offshore wind and wave power," *International Journal of Marine Energy*, vol. 17, pp. 98–109, 2017.

[8] O. Langhamer, K. Haikonen, and J. Sundberg, "Wave power—sustainable energy or environmentally costly? a review with special emphasis on linear wave energy converters," *Renewable and Sustainable Energy Reviews*, vol. 14, no. 4, pp. 1329–1335, 2010.

[9] A. E. Copping, L. G. Hemery, D. M. Overhus, L. Garavelli, M. C. Freeman, J. M. Whiting, A. M. Gorton, H. K. Farr, D. J. Rose, and L. G. Tugade, "Potential environmental effects of marine renewable energy development—the state of the science," *Journal of Marine Science and Engineering*, vol. 8, no. 11, p. 879, 2020.

[10] B. Guo and J. V. Ringwood, "A review of wave energy technology from a research and commercial perspective," *IET Renewable Power Generation*, vol. 15, no. 14, pp. 3065–3090, 2021.

[11] A. Trueworthy and B. DuPont, "The wave energy converter design process: Methods applied in industry and shortcomings of current practices," *Journal of Marine Science and Engineering*, vol. 8, no. 11, p. 932, 2020.

[12] J. V. Ringwood, G. Bacelli, and F. Fusco, "Energy-maximizing control of wave-energy converters: The development of control system technology to optimize their operation," *IEEE control systems magazine*, vol. 34, no. 5, pp. 30–55, 2014.

[13] N. Faedo, S. Olaya, and J. V. Ringwood, "Optimal control, mpc and mpc-like algorithms for wave energy systems: An overview," *IFAC Journal of Systems and Control*, vol. 1, pp. 37–56, 2017.

[14] M. Göteman, M. Giassi, J. Engström, and J. Isberg, "Advances and challenges in wave energy park optimization—a review," *Frontiers in Energy Research*, vol. 8, p. 26, 2020.

[15] B. Robertson, C. Hiles, E. Luczko, and B. Buckham, "Quantifying wave power and wave energy converter array production potential," *International Journal of Marine Energy*, vol. 14, pp. 143–160, 2016.

[16] K. Ruehl and D. Bull, "Wave energy development roadmap: Design to commercialization," in *2012 Oceans*, 2012, pp. 1–10.

[17] J. Hodges, J. Henderson, L. Ruedy, M. Soede, J. Weber, P. Ruiz-Minguela, H. Jeffrey, E. Bannon, M. Holland, R. Maciver *et al.*, "An international evaluation and guidance framework for ocean energy technology," International Energy Agency - Ocean Energy Systems (IEA-OES), Lisbon, Portugal, Tech. Rep., 2021.

[18] N. Faedo, Y. Peña-Sanchez, D. García-Violini, F. Ferri, G. Mattiazzo, and J. V. Ringwood, "Experimental assessment and validation of energy-maximising moment-based optimal control for a prototype wave energy converter," *Control Engineering Practice*, vol. 133, p. 105454, 2023.

[19] R. H. Hansen and M. M. Kramer, "Modelling and control of the wavestar prototype," in *9th European Wave and Tidal Energy Conference (EWTEC), Southampton*, 2011, pp. 1–10.

[20] "VTI ingeniería," https://www.vtisl.com/en/test-systems/wave-laboratories/, accessed: 2023-02-10.

TABLE II
VARIABLES FOR TESTS 1 TO 4, CONTAINED WITHIN THE DATASET.

	Name	Description	Units	Dim.
All tests	*time*	Time vector (common to all variables)	s	$1 \times N_t$
Test 1	*waveElevation_UD*	Wave elevation in all probe locations (1 to 19)	m	$19 \times N_t$
Test 2	*waveElevation_WE*	Wave elevation in probes 1 to 14	m	$14 \times N_t$
	excitationForce_WE	Wave excitation force (w.r.t. point **B**)	N	$N_d \times N_t$
	excitationTorque_WE	Wave excitation torque (w.r.t. point **A**)	Nm	$N_d \times N_t$
Test 3	*waveElevation_UM*	Wave elevation in probes 1 to 14	m	$14 \times N_t$
	motorPos_UM	Position of linear motor (as measured by motor driver)	m	$N_d \times N_t$
	laserPos_UM	Position of linear motor (as measured by laser sensor)	m	$N_d \times N_t$
	motorVel_UM	Velocity of linear motor (as estimated by motor driver)	m/s	$N_d \times N_t$
	accelerometerAcc_UM	Acceleration w.r.t. point **E** (as measured by accelerometer)	m/s^2	$N_d \times N_t$
	angularPos_UM	Angular position w.r.t. point **A**	rad	$N_d \times N_t$
	angularVel_UM	Angular velocity w.r.t. point **A** (output of KF)	rad/s	$N_d \times N_t$
	angularAcc_UM	Angular acceleration w.r.t. point **A**	rad/s^2	$N_d \times N_t$
Test 4	*waveElevation_CM_P*	Wave elevation in probes 1 to 14 under P control	m	$14 \times N_t$
	motorPos_UM_P	Position of linear motor (as measured by motor driver) under P control	m	$N_d \times N_t$
	laserPos_UM_P	Position of linear motor (as measured by laser sensor) under P control	m	$N_d \times N_t$
	motorVel_UM_P	Velocity of linear motor (as estimated by motor driver) under P control	m/s	$N_d \times N_t$
	accelerometerAcc_UM_P	Acceleration w.r.t. point **E** (as measured by accelerometer) under P control	m/s^2	$N_d \times N_t$
	angularPos_UM_P	Angular position w.r.t. point **A** under P control	rad	$N_d \times N_t$
	angularVel_UM_P	Angular velocity w.r.t. point **A** (output of KF) under P control	rad/s	$N_d \times N_t$
	angularAcc_UM_P	Angular acceleration w.r.t. point **A** under P control	rad/s^2	$N_d \times N_t$
	controlForce_UM_P	Requested control force (reference to motor driver) w.r.t. point **B** under P control	N	$N_d \times N_t$
	controlTorque_UM_P	Requested control torque (reference to motor driver) w.r.t. point **A** under P control	Nm	$N_d \times N_t$
	waveElevation_CM_PI	Wave elevation in probes 1 to 14 under PI control	m	$14 \times N_t$
	motorPos_UM_PI	Position of linear motor (as measured by motor driver) under PI control	m	$N_d \times N_t$
	laserPos_UM_PI	Position of linear motor (as measured by laser sensor) under PI control	m	$N_d \times N_t$
	motorVel_UM_PI	Velocity of linear motor (as estimated by motor driver) under PI control	m/s	$N_d \times N_t$
	accelerometerAcc_UM_PI	Acceleration w.r.t. point **E** (as measured by accelerometer) under PI control	m/s^2	$N_d \times N_t$
	angularPos_UM_PI	Angular position w.r.t. point **A** under PI control	rad	$N_d \times N_t$
	angularVel_UM_PI	Angular velocity w.r.t. point **A** (output of KF) under PI control	rad/s	$N_d \times N_t$
	angularAcc_UM_PI	Angular acceleration w.r.t. point **A** under PI control	rad/s^2	$N_d \times N_t$
	controlForce_UM_PI	Requested control force (reference to motor driver) w.r.t. point **B** under PI control	N	$N_d \times N_t$
	controlTorque_UM_PI	Requested control torque (reference to motor driver) w.r.t. point **A** under PI control	Nm	$N_d \times N_t$

[21] J. Ringwood, F. Ferri, N. Tom, K. Ruehl, N. Faedo, G. Bacelli, Y.-H. Yu, and R. G. Coe, "The wave energy converter control competition: Overview," in *International Conference on Offshore Mechanics and Arctic Engineering*, vol. 58899. American Society of Mechanical Engineers, 2019, p. V010T09A035.

[22] P. Tona, G. Sabiron, H.-N. Nguyen, A. Mérigaud, and C. Ngo, "Experimental assessment of the ifpen solution to the wec control competition," in *International Conference on Offshore Mechanics and Arctic Engineering*, vol. 84416. American Society of Mechanical Engineers, 2020, p. V009T09A023.

[23] A. S. Zurkinden, F. Ferri, S. Beatty, J. P. Kofoed, and M. Kramer, "Non-linear numerical modeling and experimental testing of a point absorber wave energy converter," *Ocean Engineering*, vol. 78, pp. 11–21, 2014.

[24] S. Heo and W. Koo, "Dynamic response analysis of a wavestar-type wave energy converter using augmented formulation in korean nearshore areas," *Processes*, vol. 9, no. 10, p. 1721, 2021.

[25] A. Babarit, "On the park effect in arrays of oscillating wave energy converters," *Renewable Energy*, vol. 58, pp. 68–78, 2013.

[26] A. Falcao, "Wave-power absorption by a periodic linear array of oscillating water columns," *Ocean Engineering*, vol. 29, no. 10, pp. 1163–1186, 2002.

[27] A. De Andrés, R. Guanche, L. Meneses, C. Vidal, and I. Losada, "Factors that influence array layout on wave energy farms," *Ocean Engineering*, vol. 82, pp. 32–41, 2014.

[28] W. Chen, F. Gao, X. Meng, and J. Fu, "Design of the wave energy converter array to achieve constructive effects," *Ocean Engineering*, vol. 124, pp. 13–20, 2016.

[29] D. E. Hasselmann, M. Dunckel, and J. Ewing, "Directional wave spectra observed during jonswap 1973," *Journal of physical oceanography*, vol. 10, no. 8, pp. 1264–1280, 1980.

[30] R. Kurnia and G. Ducrozet, *NEMOH V3.0 User Manual*, Ecole Centrale de Nantes.

[31] M. K. Ochi, *Ocean Waves: The Stochastic Approach*, ser. Cambridge Ocean Technology Series. Cambridge University Press, 1998.